

2-15-2000

Phase formation in hypostoichiometric $\text{Sm}_2\text{Fe}_{17}$ alloys modified with Ti and C

Jeffrey E. Shield

University of Nebraska - Lincoln, jshield@unl.edu

B.E. Meacham

University of Utah, Salt Lake City, Utah

Follow this and additional works at: <http://digitalcommons.unl.edu/cmrafacpub>



Part of the [Nanoscience and Nanotechnology Commons](#)

Shield, Jeffrey E. and Meacham, B.E., "Phase formation in hypostoichiometric $\text{Sm}_2\text{Fe}_{17}$ alloys modified with Ti and C" (2000). *Faculty Publications from Nebraska Center for Materials and Nanoscience*. 78.

<http://digitalcommons.unl.edu/cmrafacpub/78>

This Article is brought to you for free and open access by the Materials and Nanoscience, Nebraska Center for (NCMN) at DigitalCommons@University of Nebraska - Lincoln. It has been accepted for inclusion in Faculty Publications from Nebraska Center for Materials and Nanoscience by an authorized administrator of DigitalCommons@University of Nebraska - Lincoln.

Phase formation in hypostoichiometric $\text{Sm}_2\text{Fe}_{17}$ alloys modified with Ti and C

J. E. Shield^{a)} and B. E. Meacham

Department of Materials Science and Engineering, University of Utah, Salt Lake City, Utah 84112

(Received 15 July 1999; accepted for publication 1 November 1999)

The phase formation, crystallization products, microstructure, and magnetic behavior of Fe-rich Sm-Fe alloys modified with Ti and C have been determined. Alloys of nominal composition $(\text{Sm}_{0.11-x}\text{Fe}_{0.89+x})_{94}\text{Ti}_3\text{C}_3$ with $x=0, 0.02,$ and 0.04 were produced by melt spinning. Crystalline phases observed included SmFe_7 and $\alpha\text{-Fe}$ and an increasing amorphous fraction was observed with increasing x . Upon crystallization the amorphous fraction converted to $\text{Sm}_2\text{Fe}_{17}$ and $\alpha\text{-Fe}$, with a grain size of 30 nm for the sample with $x=0.02$. The magnetic measurements of nitrated alloys revealed a remanent ratio above 0.5 for $x=0$ and 0.02, although the coercivity was rather low.

© 2000 American Institute of Physics. [S0021-8979(00)01804-1]

Interstitially modified rare earth compounds, notably $\text{Sm}_2\text{Fe}_{17}\text{N}_y$, possess excellent hard magnetic properties and as such have generated tremendous interest.^{1,2} There has also been a great deal of attention on “exchange-coupled” or “spring-type” magnets that combine attributes of hard and soft magnetic phases. The $\text{Sm}_2\text{Fe}_{17}\text{N}_y/\alpha\text{-Fe}$ exchange coupled permanent magnets are expected to have excellent hard magnetic properties and elevated temperature potential.³ To fully realize the potential of high energy product interstitial compounds, it is necessary to understand phase relationships and microstructures in Sm-Fe-based systems.

In the Sm-Fe system, rapid solidification by melt spinning results in crystalline and amorphous structures depending on Sm content. The glass-forming region was initially reported to be above 17 at. % Sm,⁴ although in subsequent work a glassy structure was found to form at compositions closer to 12 at. % Sm.⁵ Very little glass formation was observed at the $\text{Sm}_2\text{Fe}_{17}$ stoichiometry (10.5 at. % Sm), even at extremely high wheel speeds.^{6,7} Crystallization products of glass-forming Sm-Fe alloys depend on composition, with $\alpha\text{-Fe}$, SmFe_2 , and SmFe_7 forming at compositions less than 17 at. % Sm.^{3,6} SmFe_7 has the TbCu_7 structure in which the Fe-Fe dumbbells lack the long-range order present in the $\text{Th}_2\text{Zn}_{17}$ -type $\text{Sm}_2\text{Fe}_{17}$ structure. Crystalline phase formation during rapid solidification at lower Sm contents generally includes $\alpha\text{-Fe}$, SmFe_7 , and SmFe_2 .^{5,8-10} The scale of the microstructure of melt spun Sm-Fe near the $\text{Sm}_2\text{Fe}_{17}$ stoichiometry ranged from 300 to 800 nm depending on solidification conditions.⁹

Exchange coupled magnets critically depend on the phase constitution, distribution, and scale. For exchange coupling to dominate over bulk effects, the individual hard and soft grains must be on the nanometer scale, optimally with the dimension of the soft phase approximately twice the domain wall thickness of the hard phase. Nanoscale $\text{Nd}_2\text{Fe}_{14}\text{B}/\alpha\text{-Fe}$ microstructures resulting in exchange cou-

pling have been produced by melt processing,^{11,12} mechanical alloying,^{13,14} and mechanical milling.¹⁵ However, nanoscale $\text{Sm}_2\text{Fe}_{17}\text{N}_x/\alpha\text{-Fe}$ microstructures have only been produced via mechanical milling¹⁶ as solidification processing, even at high rates, produces microstructures too coarse for effective exchange coupling.⁹

Selective alloying can result in a significant reduction in microstructural scale and enhance glass-forming characteristics of a system. Branagan and McCallum¹⁷ have shown the effectiveness of the compound addition of Ti and C in improving the glass formability of Nd-Fe-B alloys, and Shield *et al.*⁹ have similarly found an order of magnitude reduction in grain size for TiC-modified Sm-Fe alloys at the $\text{Sm}_2\text{Fe}_{17}$ stoichiometry. In this article, we report the phase formation and microstructures in Fe-rich Sm-Fe alloys modified with Ti and C in order to develop solidification-processed $\text{Sm}_2\text{Fe}_{17}\text{N}_x/\alpha\text{-Fe}$ exchange coupled magnetic materials.

Samples with nominal compositions of $(\text{Sm}_{0.11-x}\text{Fe}_{0.89+x})_{94}\text{Ti}_3\text{C}_3$ with $x=0, 0.02,$ and 0.04 were arc melted from high purity elemental constituents. The arc melted ingots were then melt spun at a tangential velocity of 40 m/s utilizing a copper wheel. Samples were characterized by x-ray diffraction utilizing a Philips $\theta-2\theta$ diffractometer and by transmission electron microscopy with a JEOL 2000FXII transmission electron microscope. Samples were annealed after wrapping in Ta foil and sealing in quartz capsules under high purity Ar. Nitrogenation was done at 475 °C for 4 h in flowing N_2 . The nitrogenation was confirmed by x-ray diffraction, which revealed peak shifts characteristic of the presence of interstitial nitrogen in the $\text{Sm}_2\text{Fe}_{17}$ structure. The magnetic properties of nitrated ribbon samples were measured with a Quantum Design superconducting quantum interference device (SQUID) magnetometer with a maximum field of 5.5 T. ribbon rather than powder samples were measured so that demagnetization factors could be neglected.

The phase formation in $(\text{Sm}_{0.11-x}\text{Fe}_{0.89+x})_{94}\text{Ti}_3\text{C}_3$ as a function of x was determined by x-ray diffraction. With $x=0$, the primary phase observed indexed to the TbCu_7 -type SmFe_7 structure, with no evidence of the long-range-ordered

^{a)} Author to whom correspondence should be addressed; electronic mail: jeffrey.shield@mse.utah.edu

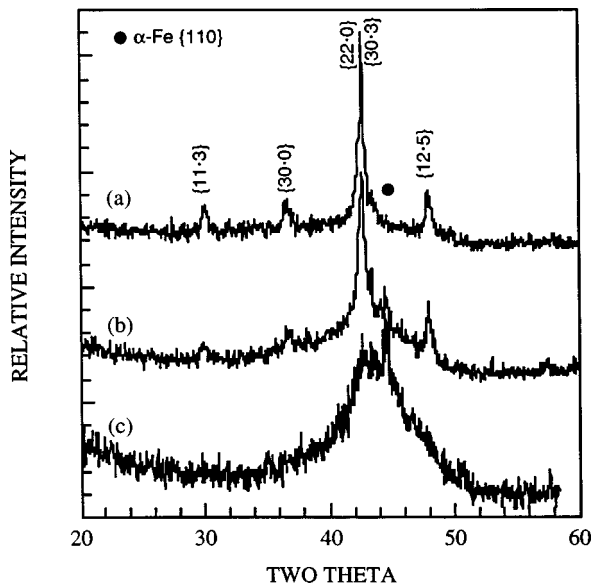


FIG. 1. X-ray diffraction patterns of as-solidified $(\text{Sm}_{11-x}\text{Fe}_{89+x})_{94}\text{Ti}_3\text{C}_3$ with x equal to (a) 0, (b) 0.02, and (c) 0.04.

$\text{Sm}_2\text{Fe}_{17}$ structure (Fig. 1). Additionally, a small diffuse “hump” was observed, indicative of a small fraction of an amorphous phase. With $x=0.02$, peaks from SmFe_7 were again observed, as well as the $\{110\}$ peak from $\alpha\text{-Fe}$. The diffuse peak was of greater intensity, indicative of a larger fraction of amorphous material in this sample as compared with $x=0$. With $x=0.04$, the sample was largely amorphous with an $\alpha\text{-Fe}$ crystalline component; no SmFe_7 was observed. Thus, the addition of Ti and C has extended the glass-forming region to a much lower Sm content than previously observed.

The crystallization products were determined by annealing the samples at 600°C for 10 min. At $x=0$, very little change in the x-ray diffraction pattern was observed as only

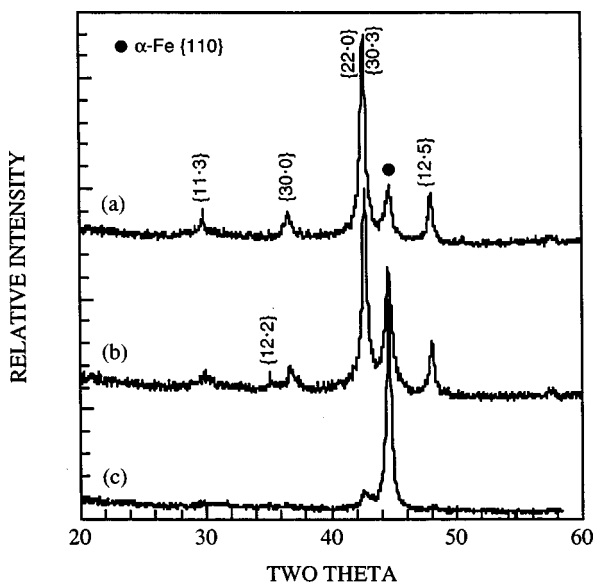


FIG. 2. X-ray diffraction patterns of $(\text{Sm}_{11-x}\text{Fe}_{89+x})_{94}\text{Ti}_3\text{C}_3$ after annealing at 600°C for 10 min for x equal to (a) 0, (b) 0.02, and (c) 0.04.

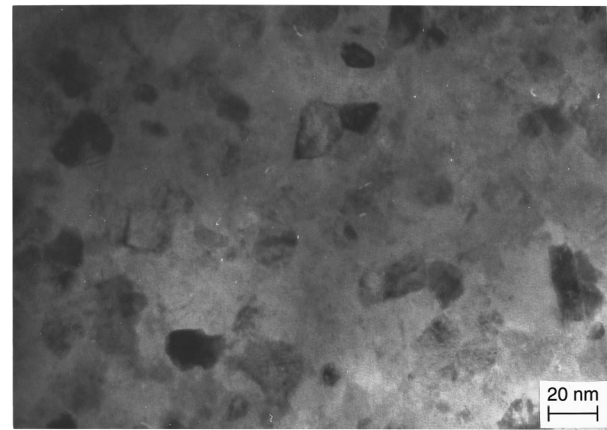


FIG. 3. Bright field transmission electron microscopy micrograph of $(\text{Sm}_{11-x}\text{Fe}_{89+x})_{94}\text{Ti}_3\text{C}_3$ with $x=0.02$ after annealing at 600°C for 10 min.

a small fraction of the sample crystallized from the amorphous state [Fig. 2(a)]. At $x=0.02$ and 0.04, the x-ray diffraction patterns no longer possess the diffuse peak associated with the amorphous phase fraction. For $x=0.02$, the amorphous fraction crystallized to the $\text{Sm}_2\text{Fe}_{17}$ structure with Fe–Fe dumbbells possessing long-range order, indicated by the presence of the $\{12\cdot 2\}$ superlattice peak [Fig. 2(b)]. Also, an increased amount of $\alpha\text{-Fe}$ was observed. For $x=0.04$, the crystallized sample contained predominantly $\alpha\text{-Fe}$, with a small fraction of presumably $\text{Sm}_2\text{Fe}_{17}$ [Fig. 2(c)], although the fraction of this phase was too low to observe the superlattice reflections. As for $x=0.02$, crystallization resulted in an increased amount of $\alpha\text{-Fe}$, indicating that the amorphous fraction crystallized to both $\text{Sm}_2\text{Fe}_{17}$ and $\alpha\text{-Fe}$. It should be noted that at equilibrium the Lever rule predicts approximately 33% $\alpha\text{-Fe}$ for a composition with $x=0.04$. The crystallized sample of Fig. 2(c) contains significantly more than 33% $\alpha\text{-Fe}$ for two reasons: (1) the as-solidified material is not in equilibrium and contains primary $\alpha\text{-Fe}$. Only the remaining amorphous component will crystallize to an equilibrium phase distribution. (2) Loss of Sm

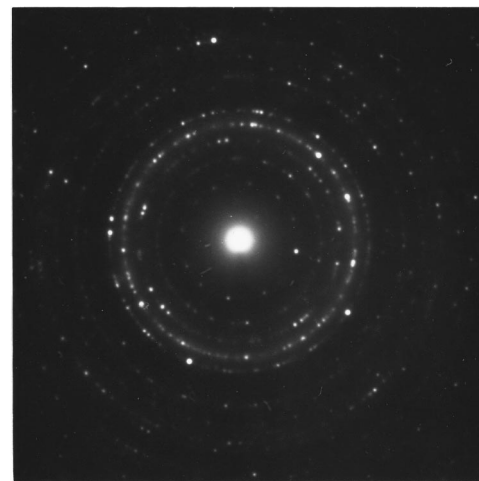


FIG. 4. Selected area electron diffraction pattern of the region shown in Fig. 3. All rings indexed to the $\text{Sm}_2\text{Fe}_{17}$ structure with no evidence of $\alpha\text{-Fe}$.

TABLE I. Magnetic properties of $(\text{Sm}_{0.11-x}\text{Fe}_{0.89+x})_{94}\text{Ti}_3\text{C}_3$. The saturation magnetization used was the magnetization measured at 48 kG.

x	H_c (Oe)	$4\pi M_r/4\pi M_s$
0	602	0.53
0.02	250	0.51
0.04	50	0.36

during arc melting and melt spinning would alter the true composition to be more Fe rich.

The crystallized microstructure for $x=0.02$ was examined by transmission electron microscopy. The microstructure consisted of equiaxed grains on the order of 30 nm (Fig. 3). The selected area diffraction pattern of this region revealed reflections corresponding only to the $\text{Sm}_2\text{Fe}_{17}$ phase; no α -Fe reflections were observed (Fig. 4). The Fe is likely predominantly in regions where it formed as a primary phase from the liquid. Thus, a highly variable microstructure with regions of primary Fe in addition to the fine, crystallized $\text{Sm}_2\text{Fe}_{17}$ grains exists.

The idea of a variable microstructure is substantiated by the magnetic properties of the nitrided samples. While reasonably high remanent ratios (above 0.5) were observed for the nitrided samples with $x=0$ and 0.02, the coercivity was only on the order of 600 Oe for $x=0$ (Table I). The low coercivity may result from a nonuniform microstructure where coarse, decoupled α -Fe grains enable the demagnetization process. Further work is under way to gain a better understanding of the microstructures in order to improve the magnetic properties.

$(\text{Sm}_{0.11-x}\text{Fe}_{0.89+x})_{94}\text{Ti}_3\text{C}_3$ alloys show a greater propensity for the formation of an amorphous phase fraction with increasing x . Essentially a two-phase mixture of α -Fe and the amorphous phase was observed at $x=0.04$. At $x=0$ and 0.02, α -Fe, SmFe_7 and the amorphous phase were observed,

with a greater amount of amorphous phase at $x=0.02$. Crystallization products included α -Fe and $\text{Sm}_2\text{Fe}_{17}$. The microstructure of the crystallized material with $x=0.02$ consisted of nanocrystalline grains on the order of 30 nm. The magnetic properties of the corresponding nitrided samples had a high remanent ratio and low coercivity.

The authors are grateful for support from the National Science Foundation through Grant No. DMR97-14946. The authors are also extremely grateful to K. W. Dennis of Ames Laboratory for the magnetic measurements.

- ¹J. M. D. Coey and H. Sun, *J. Magn. Magn. Mater.* **87**, L251 (1990).
- ²Y.-N. Wei, K. Sun, H. Bo-Ping, Y.-Z. Wang, X. L. Rao, G. C. Liu, Y. B. Fen, and J. X. Zhang, *J. Alloys Compd.* **194**, 9 (1993).
- ³T. Schrefl and J. Fidler, *J. Magn. Magn. Mater.* **157/158**, 331 (1996).
- ⁴P. J. Cadieu, T. D. Cheung, L. Wickranasekara, and S. H. Aly, *J. Appl. Phys.* **55**, 2611 (1984).
- ⁵Y. Xingbo, T. Miyazaki, T. Izumi, H. Saito, and M. Takahashi, *IEEE Trans. Magn.* **MAG-23**, 3104 (1987).
- ⁶M. Katter, J. Wecker, and L. Schultz, *J. Appl. Phys.* **70**, 3188 (1991).
- ⁷J. E. Shield, *J. Alloys Compd.* **291**, 222 (1999).
- ⁸F. E. Pinkerton and C. D. Fuerst, *Appl. Phys. Lett.* **60**, 2558 (1992).
- ⁹H. T. Kim, Q. F. Xiao, Z. D. Zhang, D. Y. Geng, Y. B. Kim, T. K. Kim, and H. W. Kwon, *J. Magn. Magn. Mater.* **173**, 295 (1997).
- ¹⁰J. E. Shield, C. P. Li, and D. J. Branagan, *J. Magn. Magn. Mater.* **188**, 353 (1998).
- ¹¹A. Manaf, R. A. Buckley, and H. A. Davies, *J. Magn. Magn. Mater.* **128**, 302 (1993).
- ¹²L. Withanawasam, G. C. Hadjipanayis, and R. F. Krause, *J. Appl. Phys.* **75**, 6646 (1994).
- ¹³W. Gong, G. C. Hadjipanayis, and R. F. Krause, *J. Appl. Phys.* **75**, 6649 (1994).
- ¹⁴J. Wecker, K. Schnitzke, H. Cerva, and W. Grogger, *Appl. Phys. Lett.* **67**, 563 (1995).
- ¹⁵W. F. Miao, J. Ding, P. G. McCormick, and R. Street, *J. Alloys Compd.* **240**, 200 (1996).
- ¹⁶J. Ding, P. G. McCormick, and R. Street, *J. Magn. Magn. Mater.* **124**, 1 (1993).
- ¹⁷D. J. Branagan and R. W. McCallum, *J. Magn. Magn. Mater.* **146**, 89 (1995).